Simple Statistical Testing on Existing Data of Core 39 KL SO189/2 to Reveal its Correlation Towards Sea Surface Temperature Variation

Uji Statistik Simpel pada Data Eksisting Sedimen Inti 39 KL SO189/2 untuk Mengungkap Korelasinya terhadap Variasi Suhu Muka Laut

Taufan Wiguna[1,2], Khoiril Anwar Maryunani[1], Mirzam Abdurrachman[1], Yusuf Surachman Djajadihardja[3]

[1] Program Studi Teknik Geologi, Institut Teknologi Bandung, Lb. Siliwangi, Coblong, Kota Bandung, Jawa Barat 40132

[2] Balai Teknologi Survei Kelautan, Badan Pengkajian dan Penerapan Teknologi, Gedung B.J. Habibie Lt.12, Jl. M.H. Thamrin No. 8, Menteng, Kota Jakarta Pusat, DKI Jakarta 10340

[3] Pusat Teknologi Pengembangan Sumberdaya Wilayah, Badan Pengkajian dan Penerapan Teknologi, Gedung 820 Geostech, Jl. Kw. Puspiptek, Muncul, Kota Tangerang Selatan, Banten 15314

Corresponding author: taufan.wiguna@bppt.go.id

(Received 2 October 2020; in revised form 5 October 2020; accepted 27 November 2020)

ABSTRACT: Several paleotemperature proxies using marine core sediment data have been developed and well-proven, but they need excellent laboratory handling and destructive tools. Spectrophotometer and Multi-Sensor Core Logger (MSCL) is considered rapid and non-destructive tools compared to other climate proxies. This paper enhances the correlation between existing data of spectrophotometer, MSCL, and sea surface temperature (SST) of the sediment core 39 KL from SO189/2 through a statistical test. The dataset is processed using interpolation, Pearson correlation, and K-means clustering. Pearson correlation reveals a strong correlation between spectrophotometer, MSCL, and SST. K-means clustering points out that SST is shifting from relatively colder to warmer. This study also tries to understand the source of four tephra and one terrigenous layer. It can be concluded that the spectrophotometer and MSCL have a positive correlation to SST variation.

Keywords: statistical approach, existing data of SO189/2, spectrophotometer, Multi-Sensor Core Logger, sea surface temperature

ABSTRAK: *Beberapa proksi paleotemperature menggunakan sedimen inti laut telah dikambangkan dan terbukti baik, namun membutuhkan penanganan laboratorium yang bagus dan bersifat destruktif. Spektrofotometer dan Multi Sensor Core Logger (MSCL) relatif lebih cepat dan tidak destruktif. Makalah ini membahas hubungan antara spektrofotometer, MSCL, dan temperature muka laut (SST) berdasarkan data sedimen inti 39 KL dari SO189/2 melalui pendekatan statistik. Data diolah menggunakan metode interpolasi, korelasi Pearson, dan kluster K-means. Korelasi Pearson menunjukkan korelasi kuat antara spektrofotometer, MSCL, dan SST. Kluster K-means menunjukkan pergeseran SST dari kondisi yang lebih dingin ke lebih hangat hubungan Stufi ini juga mencoba untuk memahami sumber 4 lapisan tefra dan 1 lapisan mineral terrigenous. Melalui studi ini, dapat disimpulkan bahwa spektrofotometer dan MSCL mempunyai korelasi positif terhadap variasi SST.*

Kata Kunci: *Pendekatan statistik, Data existing SO189/2, spektrofotometer, Multi Sensor Core Logger, Suhu Permukaan Laut*

INTRODUCTION

Sea Surface Temperature (SST) is among global climate change indicators and can be reconstructed based on several proxies applied to marine sediment core (Bradley, 2015). Those proxies studied in the mentioned reference are well-proven. However, the methods were destructive and need sample preparation. Rothwell (2006) summarized non-destructive techniques, rapid, and relatively cheap for sediment core analysis, including spectrophotometry (lightness/L* and chlorins/Cl), gamma-ray attenuation (GA), and magnetic susceptibility (MST), which are possible to infer climate changes (Nederbragt *et al.*, 2006; Rogerson *et al.*, 2006; Rothwell and Rack, 2006). Nederbragt *et al.* (2006), using a quantitative method, presents that L* and total organic carbon (TOC) are negatively correlated. Rogerson *et al.* (2006) indicate that low L* value is associated with Holocene dry events.

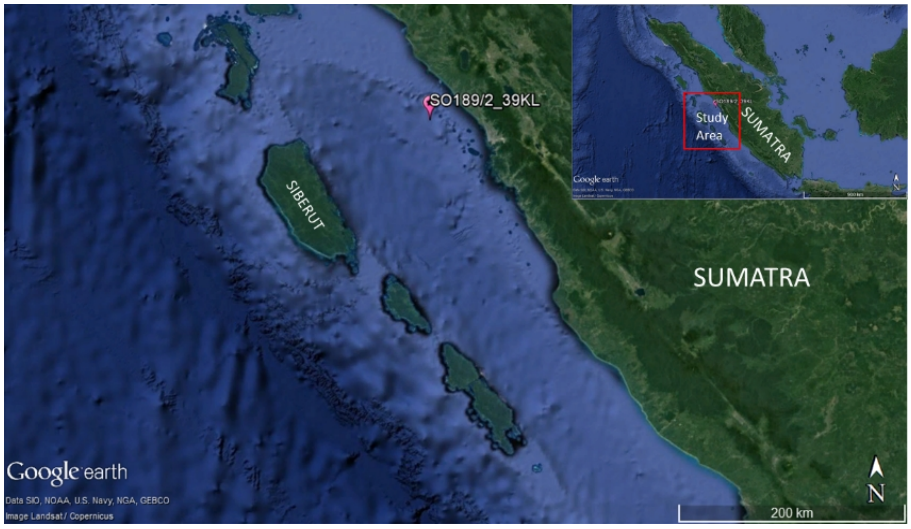

Figure 1. Location of core SO189/2_39KL

GA and MST are commonly used in core and well log analysis. In terms of paleoclimatology, GA and MST may benefit for a benchmark of orbital force and astrochronology (Huber *et al.*, 2018). Thamban *et al.* (2005) conclude that repetitive fluctuation in MST could be comparable to the glacial-interglacial cycle. Furthermore, gamma attenuation represents clay content, while magnetic susceptibility may reflect terrigenous influx. Both also deliver a hydrodynamic force and humidity environment, which exhibit a relatively positive correlation (Cao *et al.*, 2012). Hypothetically, GA and MST are positively correlated to global temperature.

Therefore, this study is conducted to reveal the correlation between the existing data of L*, Cl, GA, MST, and SST variation on the core 39 KL SO189/2 using a statistical approach. The core is collected from northern Bengkulu Basin (also known as Siberut Basin), Sumatra, Indonesia (Figure 1). Because the 39 KL SO189/2 sediment core is relatively long and has been analyzed for various datasets, we expect it to preserve relatively complete paleoclimatic data. Moreover, four tephra and a terrigenous material layer were identified within the sediment core.

METHODS AND MATERIALS

The datasets of core 39 KL are spectrophotometer, MSCL, core description which collected from SO189-2 cruise report (Wiedicke-Hombach *et al.*, 2006), age from Mohtadi *et al.* (2014b) and SST from Mohtadi *et al.* (2017). In this study, spectrophotometer data are lightness (L*) and chlorins (Cl), while MSCL data are gamma attenuation (GA) and magnetic susceptibility (MST). Spectrophotometer and MSCL data format are images, then transformed to discrete data using Graph Grabber v2.0.2 by manual picking. The datasets are processed using linear interpolation. This study workflow is described in Figure 2, and the composite dataset graph is presented in Figure 3.

Data were analyzed by Pearson correlation and K-means clustering analysis, using Minitab 18. Pearson correlation measures the strength and direction of the linear relationship between two variables, while Cluster K-means classify observation into a specified number of groups based on their similarity. K-means clustering analysis involves SST and L*, Cl, GA, and MST variables within 2 and 3 clusters. In this study, clustering number was determined based on SST variation (cooler, transition, warmer) and visualized in a 3D scatterplot by depth (z-axis), SST (y-axis), and L*/Cl/GA/MST (x-axis) to observe its variation in vertical sequence.

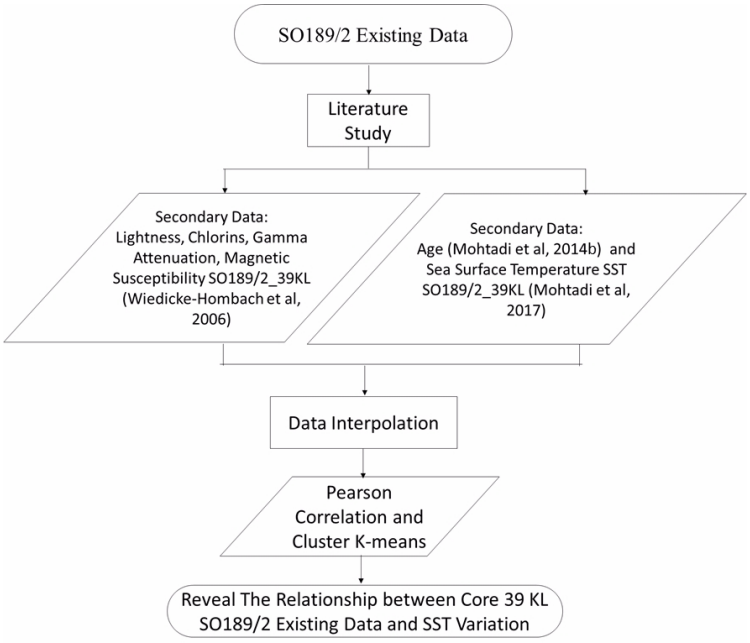

Figure 2. Flowchart of this study

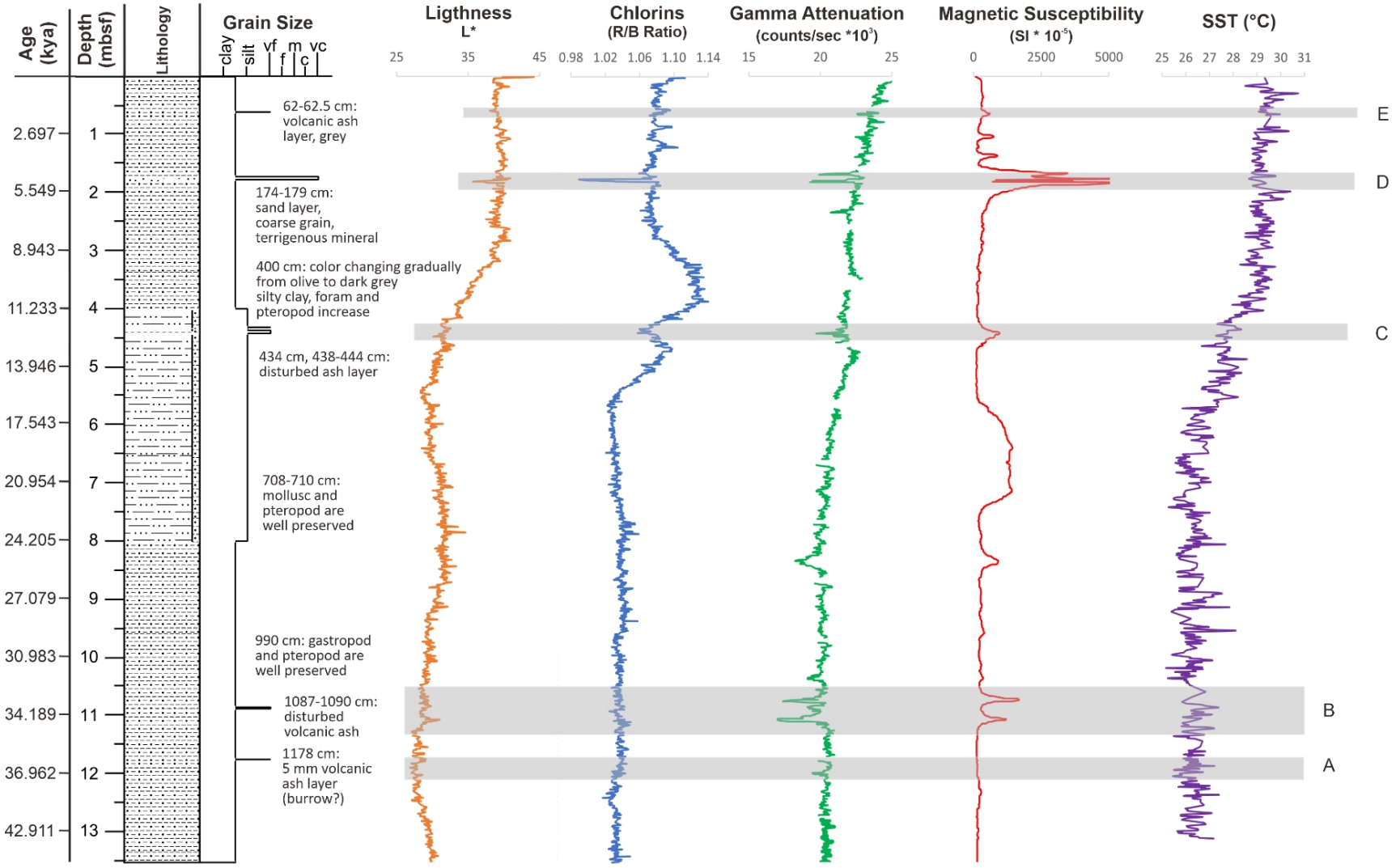

Figure 3. Composite data of core 39 KL from SO189/2. Lightness, chlorins, gamma attenuation, and magnetic susceptibility are the result of transformation from image to discrete data. SST and age are the interpolated data (modified from Wiedicke-Hombach *et al*.., 2006 and Mohtadi *et al.*, 2017). Last Glacial Maximum date according to Clark *et al.* (2009). Layer A, B, C, and E are tephra layer and Layer D is terrigenous mineral layer.

RESULTS

All data were observed from depth interval of 2 cm below seafloor (cmbsf) down to 1434 cm of the core, except for gamma attenuation (GA) started from 8 cmbsf. Two statistical analyses, Pearson correlation and K-means clustering were implemented. Pearson correlation presents a strong correlation (> 0.7) between

Table 1. Statistic Pearson correlation between SST, L*, C., GA, and MST

	SST	L*	Cl	GA
L*	0,863			
	0,000			
Cl	0,800	0,690		
	0,000	0,000		
GA	0,843	0,770	0,717	
	0,000	0,000	0,000	
MST	0,054	0,154	-0,157	-0,033
	0,048	0,000	0,000	0,227

Cell Contents
Pearson correlation
P-Value

SST, L*, Cl, and GA, in contrast with MST (Table 1). A 2D scatterplot delivered K-means clustering analysis of SST against depth and a 3D scatterplot of depth (z-axis), SST (y-axis), and L*/Cl/GA/MST (x-axis), featured in Figure 4 and 5. Using K-means clustering to SST, the boundary between clusters can be found. In SST against depth (Figure 4), the boundary between 2 cluster division is ~19.705 (675 cm), while boundaries between 3 clusters are ~27.077 kya (898 cmbsf) and ~12.628 kya (452 cmbsf).

Cluster K-means of SST, L*, Cl, and GA against depth (Figure 5) show similar patterns, either in two or three cluster divisions. Unlike the other variable, MST shows an unclear cluster pattern against SST and depth. The boundaries of 2 clusters in SST against L*, Cl, and GA are at depth 384, 453, and 530 cmbsf, respectively. In the 3 cluster divisions, two boundaries for L*, Cl, and GA are 340 and 433 cmbsf, 418 and 592 cmbsf, and 218 and 570 cmbsf. According to the cluster boundaries, it is discovered L* and GA boundaries are upper than Cl boundaries.

Composite graphic in Figure 3 is displaying all measurement variables. According to the core identification by Wiedicke-Hombach *et al.*(2006), 4 (four) tephra layers (Layer A, B, C, and E) and 1 (one) layer as terrigenous mineral (Layer D) were observed. Layer A is 0.5 mm thick at depth 1178 cmbsf. Layer B, C, and E are deposited at depth 1087-1090, 438-444, and 63-62.5 cmbsf, respectively (Figure 6). Based on depth-age interpolation, the age of Layer A, B, C, D, and E in a row are ~36.13 kya, ~34.15 kya, ~12.28 - 12.45 kya, ~4.95 - 5.20 kya, and ~1.89 kya.

Layer A at 1180 cmbsf upward indicates that all variables (L*, Cl, GA, MST, and SST), have a positive trend. Cl value slightly reduces in a specific spot of this layer (1176-1177 cmbsf), while the other variables increase. In Layer B, SST increase from 26.532 C at 1090 cmbsf to 26.723 C at 1087 cmbsf, CL and GA value indicate a similar trend, in contrast, the pattern of L* and MST is decreased upward. The SST, L*, Cl and GA of Layer C exhibit a decreasing trend from the bottom part to the upper part. The lowest L*, Cl, and GA values are at 440, 441, and 439 cmbsf, respectively. Afterward, each value increase from its lower peak to 438 cmbsf. SST is relatively constant at 442, 441, and 440 cmbsf in Layer C. Terrigenous layer (Layer D) has a significant increase of SST at 176 cmbsf, that followed by Cl and GA. Furthermore, L* increase gradually from 178 to 175 cmbsf. At 180 to 178 cmbsf, SST slightly increases from 28.662 to 28.764 C, while other variables are decreased. In contrast to the tephra layers, Layer D has an extremely high MST value, which is 4715.023 at 174 cmbsf and 5849.448 at 173 cmbsf. Layer E describes that SST at 63 to 62 cmbsf decline as well as L*, Cl, and MST, in contrast, GA are increased at that depth interval.

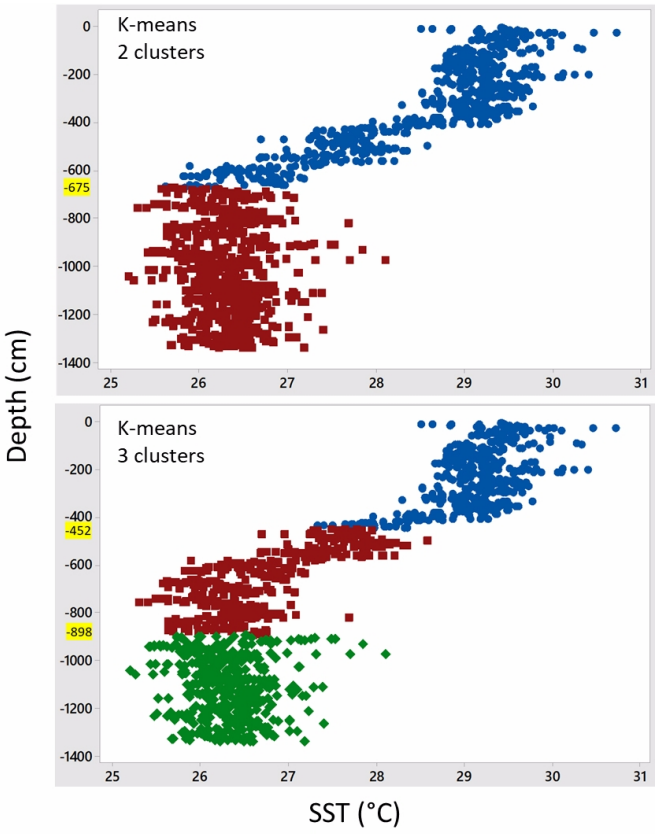

Figure 4. Scatterplot of SST against depth with K-means clustering. Each color represents a cluster. Above is scatterplot with 2 cluster divisions, while below is 3 cluster divisions.The boundary between clusters shown by yellow highlights in depth.

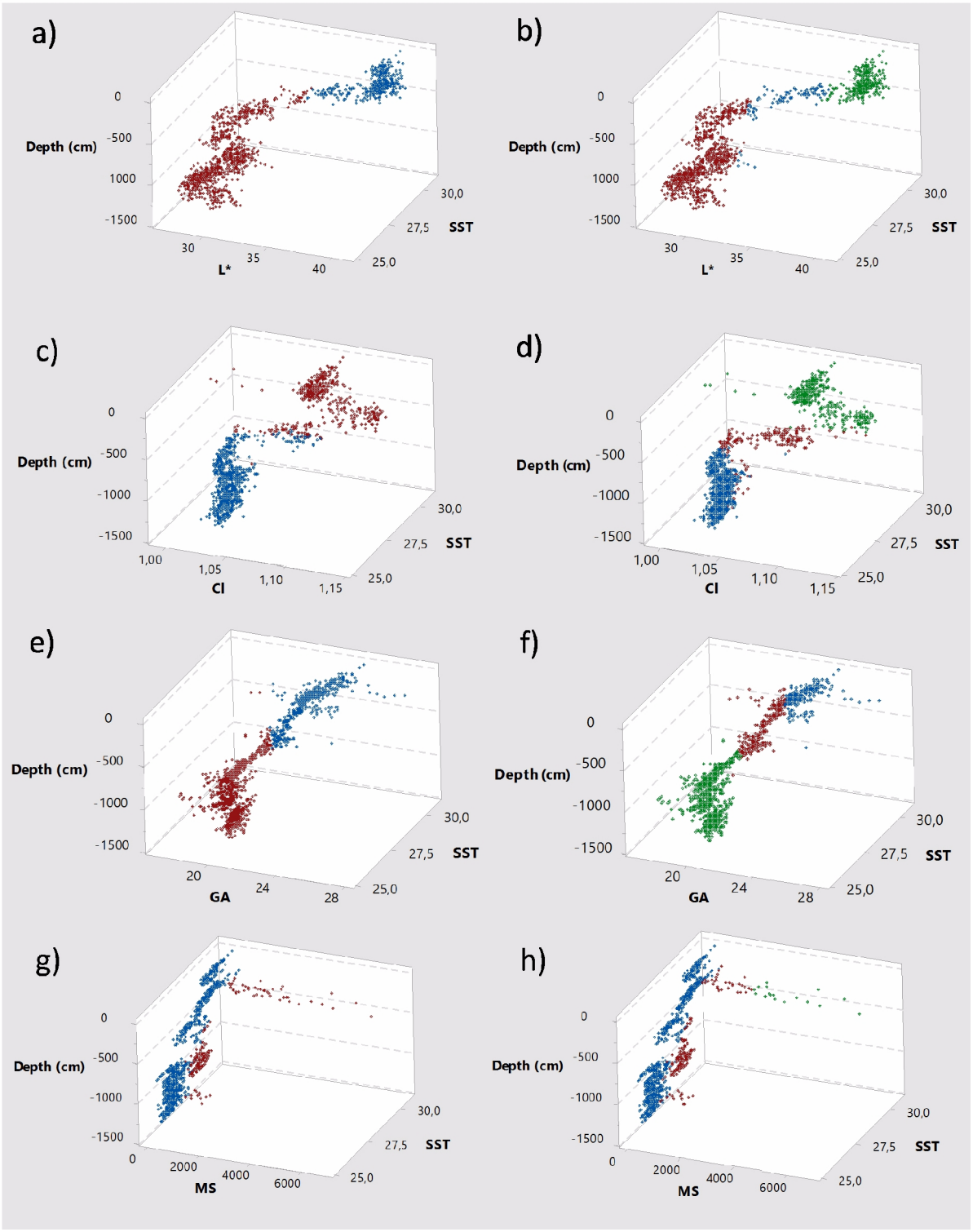

Figure 5. 3D Scatterplot with K-means clustering of SST to L*, Cl, GA, and MST. Left figures are K-means with 2 cluster divisions, while the right models are 3 clusters. Each color represents a cluster.

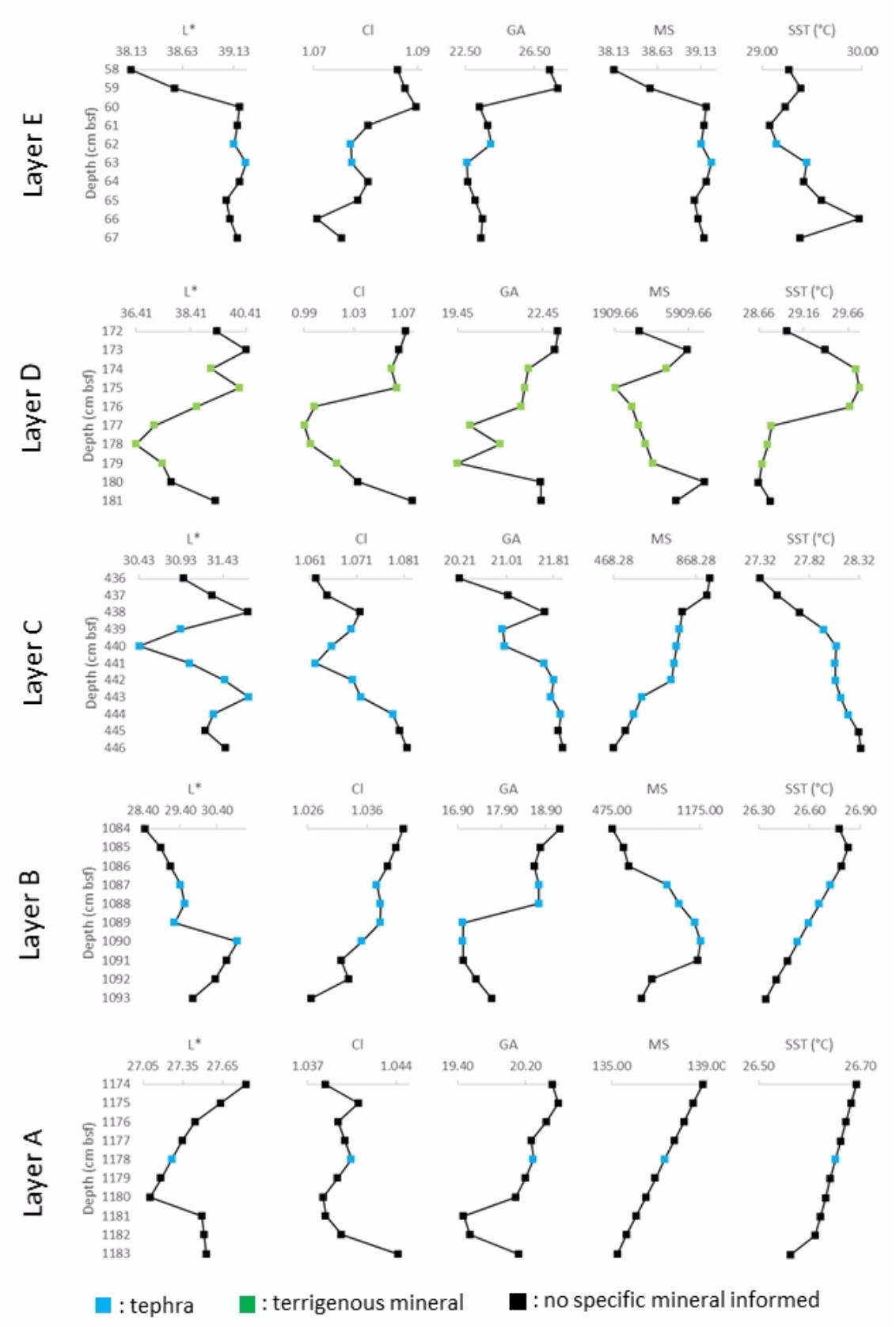

Figure 6. Composite data of tephra and terrigenous layers of core 39 KL from SO189/2. L*, Cl, GA, and MST are the result of the transformation from image to discrete data. SST is interpolated data (modified from Wiedicke-Hombach *et al.*, 2006 and Mohtadi *et al.*, 2014d, 2017)

DISCUSSIONS

Pearson correlation (Table 1) and scatterplot with K-means clustering (Figure 5) magnify the positive correlation between L*, Cl, GA, and SST variation. 2D and 3D scatterplot with K-means clustering visualize data grouping (Figure 4 and 5). Figure 5 (above) exhibits data which divided into 2 and 3 clusters, which might indicate cooler and warmer conditions. K-means scatterplot in Figure 5a, 5c, 5e, and 5g describe 2 clusters. K-means clustering of L* and SST (Figure 5a) indicate that top cluster (blue dots) at interval 2-384 cmbsf (~0.484 – 11.015 kya) represent warmer SST and bottom cluster (red dots) at interval 384-1344 cmbsf (~11.015 – 45.524 kya) represent cooler SST. Figure 5c (cluster K-means of Cl and SST) classify that the top cluster (red dots) at interval 2-453 cmbsf (~0.484 – 12.645 kya) represents warmer SST and the bottom cluster (blue dots) at interval ~453-1344 cmbsf (~12.645 – 45.523 kya) represents cooler SST. Clustering of GA and SST (Figure 5e) describes that the top cluster (blue dots) at interval 9-530 cmbsf (~0.487 – 14.662 kya) is warmer SST and the bottom cluster (red dots) at interval 530-1344 cmbsf (~14.662 – 45.524 kya) is cooler SST. Figure 5g (MST and SST) cannot be described due to no pattern revealed.

K-means scatterplot in Figure 5b, 5d, 5f, and 5h divided into 3 clusters. Figure 5b (L*, SST, and depth) classify 3 clusters at interval 2-340 cmbsf (~0.484 – 9.980 kya) as warmer SST, 340-433 cmbsf (~9.980 – 12.153 kya) as transitional SST from cooler to warmer, and 433-1344 cmbsf (~12.153 – 45.524 kya). Figure 5d (Cl, SST, and depth) describe 3 intervals as warmer SST, the transition from cooler to warmer SST, and cooler SST, at interval 2-418 cmbsf (~0.484 – 11.813 kya), 418-592 cmbsf (~11.813 – 17.125 kya), and 592-1344 cmbsf (~17.125 – 45.524 kya), respectively. K-means clustering of GA and SST (Figure 5f) show top cluster at interval 9-218 cmbsf (~487 – 5.992 kya) as warmer SST, 218-570 cmbsf (~5.992 – 16.215 kya) as transitional SST from cooler to warmer, and 570-1344 cmbsf (~16.215 – 45.662 kya) as cooler SST. Furthermore, K-mean clustering of MST and depth both at 2 cluster and 3 cluster divisions (figure 5g and 5h), the pattern cannot be described.

According to the result and SST shifting (from cooler to warmer), there is a climate event that might be related to deglaciation. Clark *et al.* (2009) analyzed that LGM occurred between 16 to 18 ka, and Mohtadi *et al.* (2014a) estimated the breaking point of deglacial warming at 18.29 ± 0.44 ka using RAMPFIT software. Those ages are near to cluster boundaries in this study. Nevertheless, the fluctuation of Cl between depth 300 and 500 cmbsf is influenced by chlorins sedimentation rate (Shankle *et al.*, 2002), also MST cannot record thin ash layer (Layer A).

To understand the four tephra layers source and one terrigenous mineral layer, they could be inferred by their age. According to Salisbury *et al.* (2012), who found six tephra unit from deep sea sediment core of Sunda Trench, Sumatra (eastern Siberut Island), the closest age to Layer A and B is V-1 (30,940 ±280 years ago), when Layer C and E have similar age to V-3 (13,610 ±630 years ago) and V-4 (1,930 ±190). Salisbury *et al.* (2012) suggest that V-3 and V-4 originated from the Central Sumatra eruption (Marapi volcano). Another possibility of the volcanic origin with a similar age to Layer A and B are Ranau (33 kya) (De Maisonneuve and Bergal-Kuvikas, 2020). We speculate that the terrigenous layer might be derived from Sumatra's channel, considering that 39 KL is located only 50 km apart from Padang.

CONCLUSSIONS

This study may conclude as follow:

1. SST, L*, Cl, and GA have a positive and a strong correlation, while MST has near zero and negative correlation to the others. It means L*, Cl, and GA on core 39 KL SO189/2 may represent SST variation, when MST spike against them.
2. L*, CL, and GA, may capture ramp and spike in SST.
3. 3D scatterplot of depth (z-axis), SST (y-axis), and L*/Cl/GA combining with K-means clustering can divide into 2 or 3 groups. Those groups represent SST zones (cooler, transition, and warmer).

ACKNOWLEDGEMENTS

The Authors would like to appreciate the contribution of all crew and scientist of SO189/2 for the data availability. The Authors would like to thank the reviewer for the intense discussion that significantly enhances this paper. This study is supported by Lembaga Pengelola Dana Pendidikan Republik Indonesia (LPDP RI) grant.

REFERENCES

Bradley, R. S., 2015. *Paleoclimatology: Reconstructing Climates of the Quaternary: Third Edition*, Elsevier Inc., 1–675. https://doi.org/10.1016/C2009-0-18310-1

Cao, L., Wang, P., Wang, J., Wang, X., and Yang, J., 2012. Changes in magnetic susceptibility and grain size of Holocene sediments of the Pearl River estuary and climate changes reflected by them. *Marine Science Bulletin* 14(2), p.70-82

Clark, P. U., Dyke, A. S., Shakun, J. D., Carlson, A. E., Clark, J., Wohlfarth, B., Mitrovica, J. X., McCabe, A. M., 2009. The Last Glacial

Maximum. *Science*, *325*(5941), 710–714. https://doi.org/10.1126/science.1172873

De Maisonneuve, C. B., dan Bergal-Kuvikas, O., 2020. Timing, magnitude and geochemistry of major Southeast Asian volcanic eruptions: identifying tephrochronologic markers, *Journal of Quaternary Science*, 35(1–2), 272–287. https://doi.org/10.1002/jqs.3181

Huber, B. T., Hobbs, R. W., Bogus, K. A., Batenburg, S. J., Brumsack, H. J., Do Monte Guerra, R., and Xu, Z., 2018. Tectonic, paleoclimate, and paleoceanographic history of high-latitude southern margins of Australia during the Cretaceous. *Integrated Ocean Drilling Program: Preliminary Reports*, (369), 1–39. https://doi.org/10.14379/iodp.pr.369.2018

Mohtadi, M., Prange, M., Oppo, D. W., De Pol-Holz, R., Merkel, U., Zhang, X., Steinke, S., Lückge, A., 2014a. North Atlantic forcing of tropical Indian Ocean climate. *Nature*, 509(7498), 76–80. https://doi.org/10.1038/nature13196

Mohtadi, M., Prange, M., Oppo, D. W., De Pol-Holz, R., Merkel, U., Zhang, X., Steinke, S., Lückge, A., 2014b. (Supplementary Table 1) Radiocarbon dating of sediment cores SO189/2_39KL, SO189/2_119KL, and SO189/2_144KL. PANGAEA, https://doi.org/10.1594/PANGAEA.833327, In supplement to: Mohtadi, M., Prange, M., Oppo, D. W., De Pol-Holz, R., Merkel, U., Zhang, X., Steinke, S., Lückge, A., 2014. North Atlantic forcing of tropical Indian Ocean climate. *Nature*, 509(7498), 76-80, https://doi.org/10.1038/nature13196

Mohtadi, M., Prange, M., Schefuß, E., and Jennerjahn, T. C., 2017. Temperatures and Mg/Ca ratios of sediment core SO189/2_039KL. PANGAEA, https://doi.org/10.1594/PANGAEA.877991, In: Mohtadi, M., Prange, M., Schefuß, E., and Jennerjahn, T. C., 2017. Late Holocene slowdown of the Indian Ocean Walker circulation. *Nat Commun* **8,** 1015. https://doi.org/10.1038/s41467-017-00855-3

Nederbragt, A. J., Dunbar, R. B., Osborn, A. T., Palmer, A., Thurow, J. W., and Wagner, T., 2006. Sediment colour analysis from digital images and correlation with sediment composition. *Geological Society Special Publication*, *267*, 113–128. https://doi.org/10.1144/GSL.SP.2006.267.01.08

Rogerson, M., Weaver, P. P. E., Rohling, E. J., Lourens, L. J., Murray, J. W., and Hayes, A., 2006. Colour logging as a tool in high-resolution palaeoceanography. *Geological Society Special Publication*, *267*, 99–112. https://doi.org/10.1144/GSL.SP.2006.267.01.07

Rothwell, R G., 2006. *New Techniques in Sediment Core Analysis. Geological Society,* London, https://doi.org/10.1144/GSL.SP.2006.267

Rothwell, R G. and Rack, F. R., 2006. New techniques in sediment core analysis: an introduction. In *New Techniques in Sediment Core Analysis*. https://doi.org/10.1144/GSL.SP.2006.267.01.01

Salisbury, M. J., Patton, J. R., Kent, A. J. R., Goldfinger, C., Djadjadihardja, Y., & Hanifa, U., 2012. Deep-sea ash layers reveal evidence for large, late Pleistocene and Holocene explosive activity from Sumatra, Indonesia. *Journal of Volcanology and Geothermal Research*, *231–232*, 61–71. https://doi.org/10.1016/j.jvolgeores.2012.03.007

Shankle, A. M., Goericke, R., Franks, P. J. S., and Levin, L. A., 2002. Chlorin distribution and degradation in sediments within and below the Arabian Sea oxygen minimum zone. *Deep Sea Research Part I: Oceanographic Research*, *49*(6), 953–969. https://doi.org/10.1016/S0967-0637(01)00077-2

Thamban, M., Naik, S. S., Mohan, R., Rajakumar, A., Basavaiah, N., D'Souza, W., and Pandey, P. C., 2005. Changes in the source and transport mechanism of terrigenous input to the Indian sector of Southern Ocean during the late Quaternary and its palaeoceanographic implications. *Journal of Earth System Science*, *114*(5), 443–452. https://doi.org/10.1007/BF02702021

Wiedicke-Hombach, M., Ardhyastuti, S., Bruns, A., Delisle, G., Georgens, R., Hermawan, T., Kanamatsu, T., Lückge, A., Mothadi, M., Mühr, P., Rahadyan, T., Riyadi, A. S., Rühlemann, C., Schippers, A., Schlömer, S., Taufik, M., Teichert, B., Vink, A., Weiss, W., Wijaya, P. H., Wöhrl, C., Zeibig, M., and Zoch, D., 2006. *SUMATRA - The hydrocarbon system of the Sumatra Forearc, cruise report BGR cruise SO189 leg 2.* https://doi.org/10.2312/cr_so189_2.